In vivo photoacoustic microscopy of human cutaneous microvasculature and a nevus

Christopher P. Favazza,[a] Omar Jassim,[b] Lynn A. Cornelius,[b] and Lihong V. Wang[a]
[a]Washington University in St. Louis, Department of Biomedical Engineering, Optical Imaging Laboratory, One Brookings Drive, Campus Box 1097, St. Louis, Missouri 63130
[b]Washington University School of Medicine, Division of Dermatology, 660 S. Euclid, Campus Box 8123, St. Louis, Missouri 63110

Abstract. In several human volunteers, photoacoustic microscopy (PAM) has been utilized for noninvasive cutaneous imaging of the skin microvasculature and a melanocytic nevus. Microvascular networks in both acral and nonacral skin were imaged, and multiple features within the skin have been identified, including the stratum corneum, epidermal-dermal junction, and subpapillary vascular plexus. Several vascular and structural differences between acral and nonacral skin were also observed in the photoacoustic images. In addition, a nevus was photoacoustically imaged, excised, and histologically analyzed. The photoacoustic images allowed for *in vivo* measurement of tumor thickness, depth, and microvasculature-values confirmed by histologic examination. The presented images demonstrate the potential of PAM to aid in the study and evaluation of cutaneous microcirculation and analysis of pigmented lesions. Through its ability to three-dimensionally image the structure and function of the microvasculature and pigmented lesions, PAM can have a clinical impact in diagnosis and assessment of systemic diseases that affect the microvasculature such as diabetes and cardiovascular disease, cutaneous malignancies such as melanoma, and potentially other skin disorders. © *2011 Society of Photo-Optical Instrumentation Engineers (SPIE)*. [DOI: 10.1117/1.3528661]

Keywords: photoacoustic microscopy; microvasculature; nevus; skin.

Paper 10385RR received Jul. 8, 2010; revised manuscript received Nov. 21, 2010; accepted for publication Nov. 30, 2010; published online Jan. 28, 2011.

1 Introduction

Photoacoustic microscopy (PAM) has many attributes that lend to *in vivo* dermatological imaging applications, such as cutaneous microvascular and pigmented lesion imaging. Particularly, these attributes include: high spatial resolution, nondestructive nature, relatively large penetration depth, and high sensitivity to oxy and deoxyhemoglobin (HbO$_2$ and HbR) and melanin. Many reports have detailed the advantages of PAM for microvascular imaging and its potential impact in a variety of clinical applications.[1–5] Such capabilities have been exploited to provide different structural and functional information and analysis of oxygen saturation (sO$_2$) (Ref. [5]), vasomotion and vasodilation,[6] and wound and burn healing.[1,7] However, the majority of PAM achievements imaging microvascular networks have been limited to small animals or phantom experiments, with far fewer reports from *in vivo* human imaging studies.[8–10] Here, we demonstrate the feasibility of PAM to image microvascular networks in human skin *in vivo*. More specifically, cutaneous blood vessel images have been obtained with dark-field PAM[11] from both the forearm and palm of a volunteer. We have utilized similar instrumentation as used and reported by Zhang et al., who also presented a photoacoustic image from a human palm.[5] The results of Zhang et al. served as a proof of principle for imaging human microvasculature in general.[5] Here we identify key anatomical structures and differentiate palm and forearm

skin from *in vivo* PAM images for the first time. In the acquired images, there are several types of identifiable structures, and significant vascular differences between skin from the palm (acral skin), and skin from the forearm (nonacral skin) are clearly visible, as would be expected for skin from these two regions of the body.

PAM is also well-suited for imaging pigmented lesions and potentially for differentiating benign lesions from melanoma. Currently, melanoma detection relies heavily on clinical suspicion. Typically, lesions are clinically evaluated for asymmetry, border irregularity, color, size (lateral dimensions), and change (evolution, lesion growth). If a lesion raises sufficient concern, it is biopsied and histologically analyzed, and a definitive diagnosis is rendered. There are a large number of pigmented lesions that may have some of the clinical characteristics of melanoma. Although it is not possible, nor clinically feasible, to excise every one of these lesions, many are nonetheless sampled and determined to be benign (i.e., unnecessary biopsies). Conversely, however, not all melanomas fully meet the clinical criteria, especially while in the earliest most curable stage, and may go undiagnosed.

For histologically confirmed melanoma, the lesion thickness, measured from the top of the epidermis, or Breslow's thickness, is the most important prognostic indicator determining propensity to metastases.[12,13] This measurement is established histologically using an ocular micrometer within the microscope, and is the distance in millimeters from the top epidermal layer (granular layer) to the deep tumor margin within the

Address correspondence to: Lihong Wang, Biomedical Engineering, Washington University in St. Louis, One Brookings Drive, Campus Box 1097, St. Louis, Missouri 63130. Tel: 314-935-6152; Fax: 314-935-7448; E-mail: lhwang@seas.wustl.edu
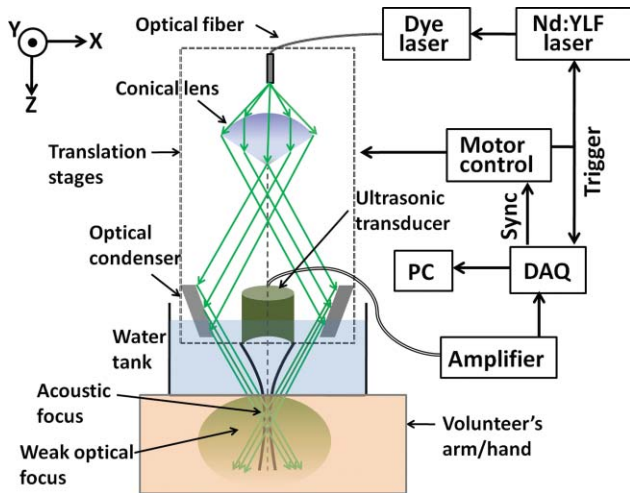
Fig. 1 Schematic of the photoacoustic microscope used in the described experiments.

dermis or subcutaneous tissue. This value is a measurement of depth of invasion and does not provide information regarding tumor size, volume, or other tumor characteristics. PAM has the potential to both match a current gold standard (Breslow thickness) and exceed it, providing three-dimensional information of the entire tumor.[5] PAM images could equip physicians with many parameters to improve early diagnosis and guide treatment plans with new prognostic indicators. Here we demonstrate the capability of PAM to characterize a pigmented lesion *in vivo*. More specifically, a nevus (i.e., a benign tumor of melanocytes) was imaged prior to excision, and the *in vivo*, three-dimensional PAM data was compared with the histology of the excised lesion.

2 Methods

2.1 Photoacoustic Microscopy

Photoacoustic (PA) images were acquired with a dark-field photoacoustic microscope assembled in the laboratory.[14] The system schematic in Fig. 1 further describes the system. A single element, broadband, focused ultrasonic transducer with a 50 MHz central frequency and 70% nominal bandwidth was utilized in the PAM system. The transducer was purchased from Panametrics (V214-BB-RM), and the focusing lens was made in the lab. Optical energy was provided by an INNOSLAB IS Nd:YLF pump laser (Edgewave GmbH, Aachen, Germany) operating in its second harmonic at a wavelength of 523 nm, with a pulse width less than 10 ns and maximum repetition rate of 3 kHz. With a dye laser (Cobra, Sirah Laser-und Plasmatechnik, Germany), the wavelength was tuned within the ranges of 561–600 nm and 680–710 nm using the following dyes, Rodamine 6G, Pyrromethene 597, and LDS 698 (Exciton, Dayton, OH). The output pulse energy from the dye laser did not exceed 3 mJ, and pulse energy incident on the surface of the target was less than 1.5 mJ. The beam was weakly focused with an optical condenser to a diameter of 2 mm in free space at the focal point. The laser energy deposited on the surface was carefully monitored and never exceeded the ANSI safety limit of 20 mJ/cm². The total time to collect an image ranged from approximately 5 to 10 min, depending on the scanning step size and field of view. All presented images were acquired with a 20 μm step size in each direction and a laser pulse repetition rate of approximately

500 Hz. All data were digitized and recorded using a commercial data acquisition card (NI PCI 5124, National Instruments Corporation, Austin, Texas) and PC.

2.2 Histology

The sample was fixed overnight in 10% neutral buffered formalin followed by paraffin embedding. Sections were cut 5 μm thick. Measurements were made using a clinically calibrated optical micrometer.

3 Results and Discussion

3.1 Skin Vasculature

3.1.1 Palm

A small section of the lower palm at the base of the thumb of a volunteer was imaged at a laser wavelength of 584 nm. An area of 8×8 mm² was scanned. The resulting images, depicted in Fig. 2, are typical of the images obtained from the palms of other volunteers in other imaging experiments. Figure 2(b) is a cross-sectional or a B-scan image. The bright pixels (bright red, for color images) in this image indicate strong PA signals generated from the surface of the skin and blood vessels below it. From this image, the boundaries of the epidermis, the stratum corneum, and the epidermal-dermal junction are easily distinguishable. Approximately 200–300 μm below the surface of the palm is the epidermal–dermal junction [Fig. 2(b)]. Large concentrations of smaller blood vessels, namely capillaries in the dermal papillae, are found in this region. Below this depth are larger vessels, presumably of the subpapillary plexus. It is well known that acral skin, like that on the palm or sole of the foot, has a much thicker epidermal layer than skin elsewhere on the body. From the PA B-scan image, the epidermal thickness is approximated as 300 μm; this measurement is within the range
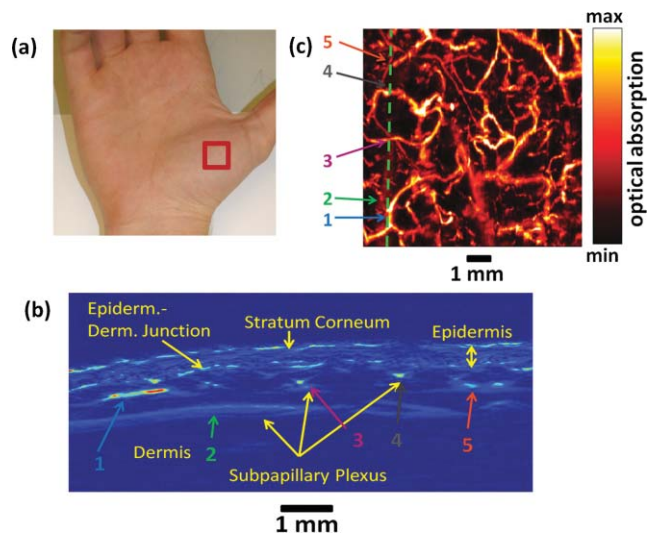
Fig. 2 (a) Photo of the palm of the volunteer. The red box indicates the imaged area 8 mm × 8 mm. (b) B-scan PA image taken along the dashed line in (c). Notable features including the stratum corneum, epidermal–dermal junction, and subpapillary blood vessels, are all labeled. Selected vessels have been labeled with color arrows for reference with the image in (c). (c) Maximum amplitude projection PA image taken from the palm using a 584 nm laser excitation wavelength. The green dashed line indicates the cross-section shown in (b). (Color online only.)
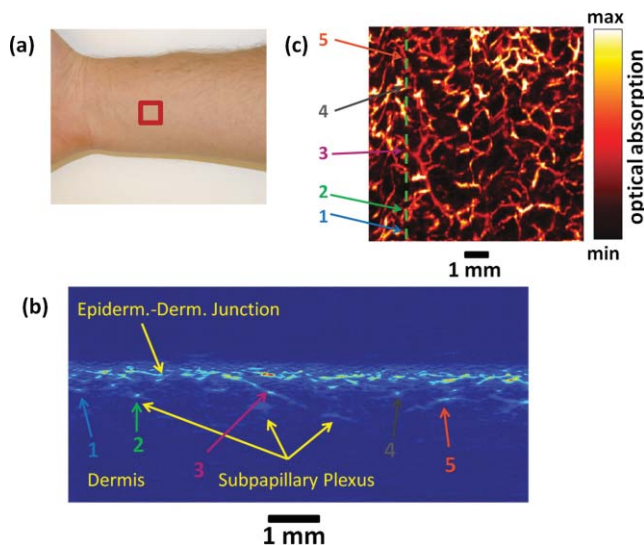
of reported values from studies that used different measurement techniques.[15,16] A maximum amplitude projection (MAP) of the 3-D image toward the skin surface is shown in Fig. 2(c), and the cross-sectional slice shown in Fig. 2(b) is indicated. To make the vessels more clearly visible, the PA signal from and above the epidermal–dermal junction and the unresolved smaller papillary capillary vessels, were removed during construction of the MAP image. The image acquisition time for this image was relatively fast (∼10 min); however, faster imaging times will reduce complications such as mechanical movement of the volunteer and enhance the spectroscopic capabilities necessary for functional measurements.

3.2 Forearm

Figure 3 shows representative images acquired with PAM from the forearm. Again, an 8×8 mm^2 area was scanned. Also, during construction of the MAP image [Fig. 3(c)] signal from and above the epidermal–dermal interface was removed to clearly show the dermal vasculature. There are clear differences between the forearm and palm images, particularly visible in the B-scan images [Figs. 2(b) and 3(b)]. The epidermal layer on the forearm is not as clearly resolved as in the images of the palm and is indistinguishable from the epidermal–dermal junction. The epidermal layer is much thinner in nonacral skin, as on the forearm, and published reports on the epidermal thickness values for nonacral skin range from tens of microns up to $<\sim 100$ μm.[15,16] Both the stratum corneum and the cellular epidermis are thinner in nonacral skin;[17–19] moreover, the stratum corneum is more compact in acral skin as compared to the less dense basket weave configuration commonly found in nonacral skin. These differences in the epidermis, particularly in the stratum corneum, likely account for the differences in the surface signals from the palm and forearm in the PAM images. In skin with a relatively thick

epidermis, such as the palm, signals generated from the epidermis itself and the dermal–epidermal junction are more discrete and easily distinguished on B-scan images. This is in contrast to skin with a thinner epidermis, in which the stratum corneum and epidermal–dermal junction are difficult to differentiate. Furthermore, the denser stratum corneum layer in the palm intrinsically absorbs more laser light and yields a stronger PA signal than the relatively uncompressed, basket woven layer in the forearm, enabling the top epidermal layer in the palm to be detected and resolved. Another difference can be seen in the epidermal–dermal interface. In forearm images, this interface has a much stronger and more diffuse signal. It is believed that the bulk of this signal is generated from the layer of capillary vessels in the dermal papillae that appears to be much denser than seen in the palm images. Microcirculation and microvascular structure are different in acral and nonacral skin. Approximately 75% of microcirculation in acral skin is through arteriovenous (AV) anastomoses, and only 25% through nutritional capillaries.[20] This is in stark contrast with microcirculation through nonacral skin, which has far fewer (or no) AV shunts; here blood circulates primarily through nutritional capillaries.[20,21] These structural and functional differences could account for the strong signal observed in the PA images of the epidermal–dermal interface in the forearm as compared to the weak signal in the palm. In essence, the greater number of perfused capillaries in the forearm generates a signal that is both stronger and broader or more diffuse than the more discrete signal from the palm images.

These imaging experiments demonstrate the potential of PAM to characterize the structure and functioning of human cutaneous microvascular networks *in vivo*. The ability to accurately image microvasculature in human skin *in vivo* can aid the study and understanding of microcirculation, in turn aiding in the diagnosis and monitoring of many cardiovascular diseases, including diabetes, renal disease, hypertension, peripheral vascular disease,[22–26] as well as vascular lesions, such as hemangiomas and angiogenesis of tumors.
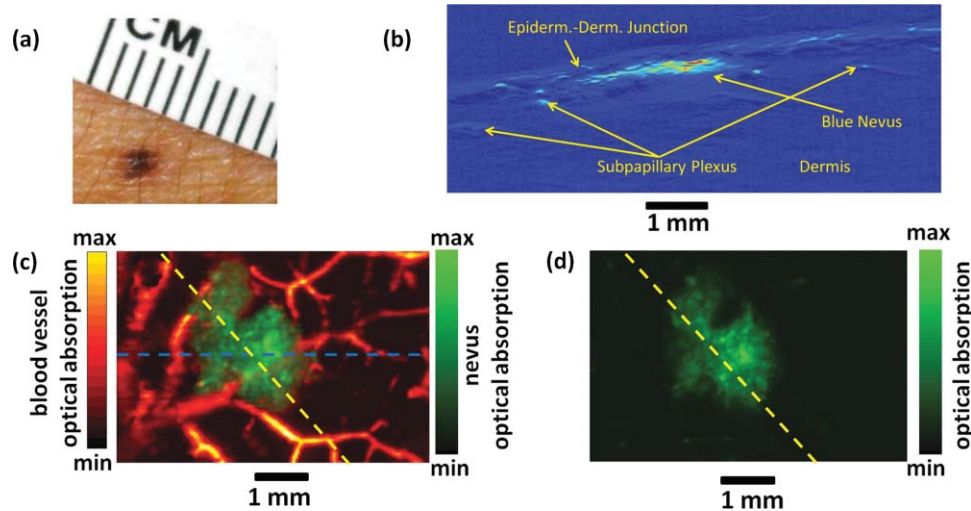
3.3 Pigmented Lesion

3.3.1 Nevus

A common blue nevus in the forearm of a volunteer is shown in Fig. 4(a). It was photoacoustically imaged and subsequently removed with a 3 mm punch biopsy, then histologically analyzed. Prior to excision, a 6 mm × 4 mm area encompassing the nevus was imaged with PAM at two different laser excitation wavelengths, 570 and 700 nm. The first wavelength, 570 nm, was chosen because it is an isosbestic wavelength for HbO$_2$ and HbR, and the signal at that wavelength can be used as a measure of total hemoglobin. At the longer excitation wavelength, 700 nm, the absorption of melanin, HbR, and HbO$_2$ is significantly weaker than at 570 nm, which enables deeper penetration of the laser light into the nevus. In the PA image acquired at 570 nm laser excitation wavelength, the surrounding microvasculature is clearly displayed, along with the nevus, in the MAP image [Fig. 4(c)]. In contrast, only the nevus and unresolved signal from some capillary vessels in the epidermal–dermal junction are visible in the PA images acquired at 700 nm [Fig. 4(d)]. The B-scan in Fig. 4(b) is a representative cross-section (along the scanning direction) of the nevus

Fig. 3 (a) Photo of the forearm of the volunteer. The red box indicates the imaged area 8 mm × 8 mm. (b) B-scan PA image taken along the dashed line in (c). Notable features, including the epidermal–dermal junction and subpapillary blood vessels, are labeled. Selected vessels have been labeled with color arrows and for reference the image in (c). (c) Maximum amplitude projection PA image taken from the forearm using a 584 nm laser excitation wavelength. The green dashed line indicates the cross-section shown in (b). (Color online only.)

Fig. 4 (a) Photo of a nevus located on the forearm of the volunteer. (b) B-scan PA image taken along the blue dashed line in (c). Notable features including the nevus, epidermal–dermal junction, and subpapillary blood vessels, are all labeled. (c) MAP image of a nevus acquired using 570 nm laser illumination. The nevus is clearly shown in "green scale," and blood vessels are shown in red. The blue dashed line indicates the cross-section shown in (b) and the yellow dashed line indicates the cross-section depicted in Fig. 5(c). (d) MAP image of a nevus acquired with a 700 nm laser excitation wavelength. The yellow line indicates the cross-section shown in Fig. 5(d). (Color online only.)

imaged with 570 nm light and shows the depth of the nevus and surrounding vessels.

Several measurements can be derived from the PA images that cannot be obtained with dermoscopy or photography, including the lesion's depth, thickness, and volume. To validate these measures, sections of the nevus were histologically analyzed. For comparison, it was necessary to select the correct "slice" of the 3-D data that corresponded to the same approximate section of the nevus in the histology section. To match histology with the PA data, the nevus was manually marked in photos from serial histology sections. The spacing between histology sections varied between 50 and 80 μm. A montage was made of the labeled photos and a MAP image of the nevus was formed from the histology data as shown in Fig. 5(a). Based on the shape of the nevus and other key features, namely a prominent hair follicle disrupting the nevus at the edge, the histology and PA MAP images were co-registered, and "slices" of the PA data that most closely matched with the corresponding histology sample were selected [Figs. 5(b)–5(d)]. Depth and thickness measurements were taken from the same position in the PA and histology data. PA data collected using 570 nm laser excitation light yielded the following measurements: 270 μm nevus thickness [Fig. 5(e)], 140 μm depth from the surface to the top of the nevus (410 μm total depth from the surface) [Fig. 5(e)], and a 2.66 mm width. The PA data collected with 700 nm laser light produced similar results: 262 μm nevus thickness [Fig. 5(f)], 135 μm depth from the surface to the top of the nevus (397 μm total depth from the surface) [Fig. 5(f)], and a 2.64 mm width. The edges of the nevus were defined as the points where the signal first exceeded two standard deviations from the average noise value. In both depth and lateral dimensions, differences in spatial measurements from both wavelengths were within the resolution of the system (15 μm axial and 45 μm lateral resolutions). These results are consistent, at least qualitatively, with the histology, which shows the nevus to be approximately 450 μm thick and located 150 μm deep below the surface

(600 μm total depth from the surface), with a width of 2.18 mm. The measurements from the PA data are justifiably different from histology because of tissue distortion during excision, formalin fixation, and dehydration/paraffin embedding that
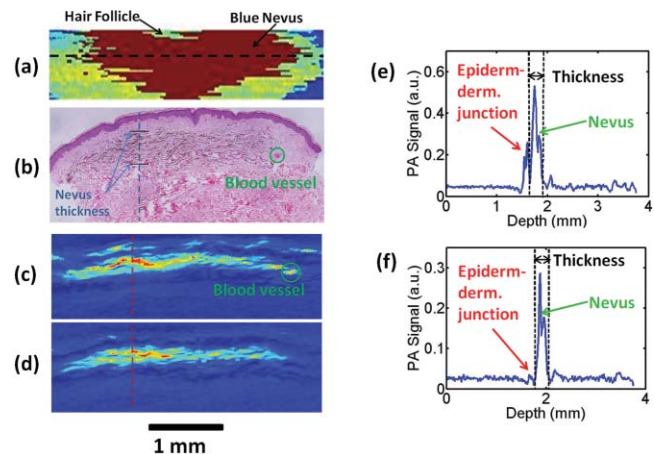

Fig. 5 (a) Maximum amplitude projection of a nevus generated from serial histology sections (top view, i.e., *en face* view, of the nevus) used to match histology with PA data. The nevus is shown in red, and a large hair follicle near the top was used to orient the image with the PA MAP image. (b) Histology section along the dashed line in (a), in which the location of the nevus thickness is indicated by the dashed line and two hash marks. A blood vessel used for orientation is circled in green. [(c) and (d)] Cross-sectional PA images of the nevus in the approximate region as (b) and are marked in Figs. 4(b)–4(c). (c) Image acquired with 570 nm laser illumination. The blood vessel circled in green matches with the vessels outlined in (b). (d) Image acquired using 700 nm laser illumination. The red dashed lines in both images (c) and (d) indicate the depth profiles shown in (e) and (f). Depth profile plots of the nevus are indicated by the dashed line in the cross-sectional images in (c) and (d). (e) Profile plot from the image acquired with a 570 nm laser excitation wavelength shows the nevus thickness to be 270 μm. (f) Profile plot from the image acquired with a 700 nm laser excitation wavelength shows the nevus thickness to be 262 μm. (Color online only.)

result in tissue shrinkage artifact. We thus anticipated that the histological measurement of lesion width would be less. Taking into account that the histology section was generated from a 3 mm punch biopsy, the width of the nevus could be scaled to the entire tissue slice, yielding a more accurate measurement. From this calibration procedure, the width of the nevus was determined to be 2.7 mm, which agrees well with PA measurements. The smaller PAM values for depth (thickness and depth) compared to histology measurements are also to be expected from distortion of the tissue along the depth direction from excision, which relaxes the lateral tension of the removed tissue and causes the tissue to collapse in the lateral directions and elongate in the depth direction.

A major concern with PA data pertains to the accuracy of the measured thickness of the lesion. From a single PA measurement, it is not necessarily guaranteed that the entire thickness of the lesion has been recorded because the PA data will not inherently indicate if light has fully penetrated the lesion. However, by imaging with two different wavelengths, it is possible to confirm that the entire thickness of the lesion was accurately recorded, if the measurements at both wavelengths are consistent. The primary absorber in a pigmented lesion is melanin and the optical absorption of melanin decays exponentially with increasing optical wavelength. Thus if one wavelength is sufficiently longer, the absorption coefficient of melanin can be an order of magnitude (or more) lower at that wavelength, which results in much deeper light penetration. The PA signal is proportional to the product of the absorption coefficient, μ_a, and the local laser fluence, which can be assumed to decay exponentially with μ_a inside a specific target (i.e., nevus, blood vessel, etc.). For example, using two wavelengths, λ_1 and λ_2, if $\mu_a^{\lambda 1} = 5 \ \mu_a^{\lambda 2}$, at a depth of $d = 1/\mu_a^{\lambda 1}$ into the target, the PA signal from λ_1 will be approximately 11 times greater than the PA signal from λ_2, or $PA(d)^{\lambda 1} \sim 11 PA(d)^{\lambda 2}$. So, if the absorption coefficient is significantly different and the initial laser fluences are roughly equivalent at the two wavelengths, similar thickness measurements will confirm that light has fully penetrated the lesion at both wavelengths and both measurements are accurate. If the thickness measurements are different, it is guaranteed that the shorter measure is inaccurate and it remains unknown if the larger value is correct or not. However, this scenario does not represent a fundamental limitation of photoacoustic imaging because utilizing longer excitation wavelengths and/or increasing the illumination intensity will enable an accurate lesion thickness measurement. The data presented here show similar thickness values using both 570 and 700 nm laser light, which validates the accuracy of the measurement. Furthermore, a blood vessel is clearly evident directly below the nevus in the PA image collected with a 570 nm laser wavelength (Video 1). The presence and detection of this blood vessel confirms that a sufficient number of photons penetrated the nevus, enough to generate the PA signal from the blood vessel. Consequently, if the nevus extended to the depth of the blood vessel seen beneath it, then a detectable PA signal should have been generated from the nevus itself at this depth. The absence of a PA signal from the nevus at the depth of this vessel suggests that the lower boundary of the nevus was detected.

With better characterization and analysis of pigmented lesions, there is great potential to improve the diagnosis and assessment of clinically atypical nevi and melanoma. Using clin-

Cross-Section 0.02 mm
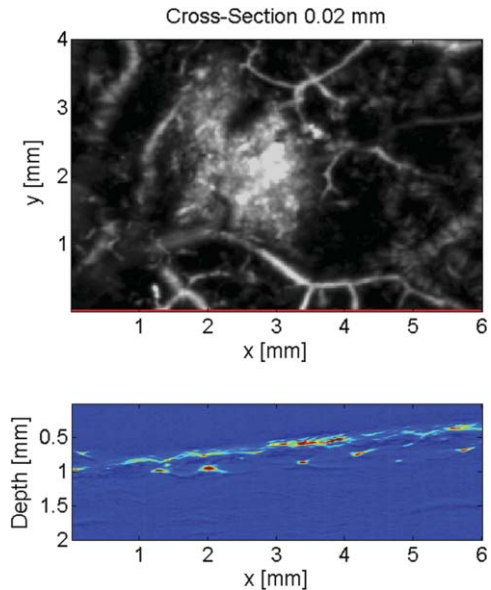
Video 1 In this video, there are two figures. The upper figure is the MAP image of the nevus and surrounding vasculature taken from the forearm of the volunteer. The lower figure shows the consecutively acquired B-scan images. The position of each B-scan image or cross-section in relation to the MAP image is indicated by the red bar on the MAP image. (QuickTime, 1 MB)
[URL: http://dx.doi.org/10.1117/1.3528661.1]

ical criteria that include asymmetry, border irregularity, color variation, diameter, and evolution, early melanomas that do not exhibit these criteria are missed. Conversely, many benign lesions (atypical nevi) may be needlessly biopsied. The use of dermoscopy has aided clinical assessment; however, this tool is useful only in the evaluation of surface characteristics and is not effectively employed by all clinicians. With PAM, additional characteristics of pigmented lesions may be noninvasively evaluated, including vasculature, lesion architecture, and 3-D symmetry. In suspected melanoma, measurements including lesion thickness and tumor volume may also be assessed *in vivo*. Once multiple pigmented lesions have been imaged, analyzed, and compared with histologic diagnoses, we anticipate that algorithms will be devised using PAM parameters to aid in the diagnosis of melanoma. This work is currently ongoing. Such information could be helpful not only in diagnosis of melanoma, but potentially in planning definitive surgery.

In conclusion, PAM has been used to collect *in vivo* images of the microvasculature and a pigmented lesion. Images of the microvasculature clearly show the structure of the vessels and the differences between vascular networks in acral and nonacral skin, and they demonstrate potential for numerous functional measurements. A benign nevus was photoacoustically imaged, biopsied, and histologically analyzed. Thickness and depth measurements of the nevus were consistent in both PA images, acquired using different laser wavelengths, and agreed well with the histology measurements, including the effect of tissue distortion during sample preparation. These results exhibit the capabilities and potential of PAM in dermatological applications.

Patients: All of the experiments were conducted in accordance with the human studies protocols approved by the Institutional Review Board at Washington University in St. Louis.

The Declaration of Helsinki protocols were followed and all volunteers freely submitted their written informed consent.

References

1. K. Aizawa, S. Sato, D. Saitoh, H. Ashida, and M. Obara, "Photoacoustic monitoring of burn healing process in rats," *J. Biomed. Opt.* **13**(6), 064020 (2008).
2. M.-L. Li, J.-T. Oh, X. Xie, G. Ku, W. Wang, C. Li, G. Lungu, G. Stoica, and L. V. Wang, "Simultaneous molecular and hypoxia imaging of brain tumors in vivo using spectroscopic photoacoustic tomography," *Proc. IEEE* **96**(3), 481–489 (2008).
3. E. W. Stein, K. Maslov, and L. V. Wang, "Noninvasive, in vivo imaging of blood-oxygenation dynamics within the mouse brain using photoacoustic microscopy," *J. Biomed. Opt.* **14**(2), 020502 (2009).
4. X. Wang, Y. Pang, G. Ku, X. Xie, G. Stoica, and L. V. Wang, "Noninvasive laser-induced photoacoustic tomography for structural and functional in vivo imaging of the brain," *Nat. Biotechnol.* **21**(7), 803–806 (2003).
5. H. F. Zhang, K. Maslov, G. Stoica, and L. V. Wang, "Functional photoacoustic microscopy for high-resolution and noninvasive in vivo imaging," *Nat. Biotech.* **24**(7), 848–851 (2006).
6. S. Hu, K. Maslov, and L. V. Wang, "Noninvasive label-free imaging of microhemodynamics by optical-resolution photoacoustic microscopy," *Opt. Express* **17**(9), 7688–7693 (2009).
7. S. Hu, K. Maslov, and L. V. Wang, "In vivo functional chronic imaging of a small animal model using optical-resolution photoacoustic microscopy," *Med. Phys.* **36**(6), 2320–2323 (2009).
8. R. G. M. Kolkman, P. J. Brands, W. Steenbergen, and T. G. van Leeuwen, "Real-time in vivo photoacoustic and ultrasound imaging," *J. Biomed. Opt.* **13**(5), 050510–050513 (2008).
9. R. G. M. Kolkman, E. Hondebrink, W. Steenbergen, T. G. van Leeuwen, and F. F. M. de Mul, "Photoacoustic imaging of blood vessels with a double-ring sensor featuring a narrow angular aperture," *J.Biomed. Opt.* **9**(6), 1327–1335 (2004).
10. J. J. Niederhauser, M. Jaeger, R. Lemor, P. Weber, and M. Frenz, "Combined ultrasound and optoacoustic system for real-time high-contrast vascular imaging in vivo," *IEEE Trans. Med. Imaging* **24**(4), 436–440 (2005).
11. K. Maslov, G. Stoica, and L. V. Wang, "In vivo dark-field reflection-mode photoacoustic microscopy," *Opt. Lett.* **30**(6), 625–627 (2005).
12. C. M. Balch, J. E. Gershenwald, S. J. Soong, J. F. Thompson, M. B. Atkins, D. R. Byrd, A. C. Buzaid, A. J. Cochran, D. G. Coit, S. Ding, A. M. Eggermont, K. T. Flaherty, P. A. Gimotty, J. M. Kirkwood, K. M. McMasters, M. C. Mihm, Jr., D. L. Morton, M. I. Ross, A. J. Sober, and V. K. Sondak, "Final version of 2009 AJCC melanoma staging and classification," *J. Clin. Oncol.* **27**(36), 6199–6206 (2009).
13. A. Breslow, "Thickness, cross-sectional areas and depth of invasion in the prognosis of cutaneous melanoma," *Ann. Surg.* **172**(5), 902–908 (1970).
14. H. F. Zhang, K. Maslov, and L. V. Wang, "In vivo imaging of subcutaneous structures using functional photoacoustic microscopy," *Nat. Protoc.* **2**(4), 797–804 (2007).
15. M. Mogensen, H. A. Morsy, L. Thrane, and G. B. E. Jemec, "Morphology and Epidermal Thickness of Normal Skin Imaged by Optical Coherence Tomography," *Dermatology (Basel, Switz.)* **217**(1), 14–20 (2008).
16. S. Nouveau-Richard, M. Monot, P. Bastien, and O. de Lacharriere, "In vivo epidermal thickness measurement: ultrasound vs. confocal imaging," *Skin Res. Technol.* **10**(2), 136–140 (2004).
17. M. Egawa, T. Hirao and M. Takahashi, "In vivo estimation of stratum corneum thickness from water concentration profiles obtained with Raman spectroscopy," *Acta. Derm. Venereol* **87**(1), 4–8 (2007).
18. M. Huzaira, F. Rius, M. Rajadhyaksha, R. R. Anderson, and S. Gonzalez, "Topographic variations in normal skin, as viewed by in vivo reflectance confocal microscopy," *J. Invest. Dermatol.* **116**(6), 846–852 (2001).
19. Z. Ya-Xian, T. Suetake, and H. Tagami, "Number of cell layers of the stratum corneum in normal skin–relationship to the anatomical location on the body, age, sex and physical parameters," *Arch. Dermatol. Res.* **291**(10), 555–559 (1999).
20. C. J. Abularrage, A. N. Sidawy, G. Aidinian, N. Singh, J. M. Weiswasser, and S. Arora, "Evaluation of the microcirculation in vascular disease," *J. Vasc. Surg.* **42**(3), 574–581 (2005).
21. J. Lundberg, L. Norgren, E. Ribbe, I. Rosen, S. Steen, J. Thorne, and B. G. Wallin, "Direct evidence of active sympathetic vasodilatation in the skin of the human foot," *J. Physiol.* **417**,437–446 (1989).
22. P. A. Carberry, A. M. Shepherd, and J. M. Johnson, "Resting and maximal forearm skin blood flows are reduced in hypertension," *Hypertension* **20**(3), 349–355 (1992).
23. K. Farkas, E. Kolossvary, Z. Jarai, J. Nemcsik, and C. Farsang, "Non-invasive assessment of microvascular endothelial function by laser Doppler flowmetry in patients with essential hypertension," *Atherosclerosis* **173**(1), 97–102 (2004).
24. F. Khan, T. A. Elhadd, S. A. Greene, and J. J. Belch, "Impaired skin microvascular function in children, adolescents, and young adults with type 1 diabetes," *Diabetes Care* **23**(2), 215–220 (2000).
25. J. Stewart, A. Kohen, D. Brouder, F. Rahim, S. Adler, R. Garrick, and M. S. Goligorsky, "Noninvasive interrogation of microvasculature for signs of endothelial dysfunction in patients with chronic renal failure," *Am. J. Physiol. Heart Circ. Physiol.* **287**(6), H2687–2696 (2004).
26. G. B. Yvonne-Tee, A. H. Rasool, A. S. Halim, and A. R. Rahman, "Noninvasive assessment of cutaneous vascular function in vivo using capillaroscopy, plethysmography and laser-Doppler instruments: its strengths and weaknesses," *Clin. Hemorheol Microcirc.* **34**(4), 457–473 (2006)